Available online at www.sciencedirect.com
ScienceDirect
Journal of the European Ceramic Society 31 (2011) 1227–1232
www.elsevier.com/locate/jeurceramsoc

Microstructure and hardness scaling in laser-processed B_4C–TiB_2 eutectic ceramics

Ryan M. White [a,b], Jamie M. Kunkle [b], Anton V. Polotai [b,1], Elizabeth C. Dickey [a,b,*]

[a] *Department of Materials Science and Engineering, Pennsylvania State University, University Park, PA 16802, United States*
[b] *Materials Research Institute, Pennsylvania State University, University Park, PA 16802, United States*

Available online 31 July 2010

Abstract

Surface layers of the pseudo-binary eutectic comprised of boron carbide (B_4C) and titanium diboride (TiB_2) were directionally solidified via direct laser irradiation in an argon atmosphere. The resulting surface eutectic layers had highly oriented lamellar microstructures, whose scale (i.e. interlamellar spacing) was controlled directly by the laser scan rate, following an inverse square root dependence for lower solidification velocities. Higher velocities (>∼4.2 mm/s) departed from this relationship, although well-ordered microstructures were still achieved. A concomitant increase in the Vickers hardness with decreasing interlamellar spacing was observed, although the trend did not correspond to traditional Hall–Petch behavior. The hardness of the eutectic composites became load-independent at indenter loads greater than 9.81 N, indicating a potential transition from plastic to fractural deformation during indentation. A Vickers hardness of 32 GPa was achieved in the highest solidification velocity samples (42 mm/s) which had interlamellar spacings of 180 nm.

Keywords: Boride; Carbide; Hardness; Composites; Eutectic

1. Introduction

Directionally solidified eutectic (DSE) ceramics are of interest for an array of thermo-mechanical applications due to their inherent thermodynamic stability and potential for improved mechanical properties relative to the monolithic end members.[1–6] In addition, the directional solidification process allows for control of the microstructural length scale, which provides some latitude in tailoring the microstructure and properties.[4,6,7] While the majority of ceramic DSE research has been devoted to oxides,[4,6] there is increasing and renewed interest in boride and carbide eutectics because of their very high eutectic temperatures (above 2000 °C), which make them attractive in ultra-high-temperature applications, and for their covalent bonding, which makes them attractive in applications requiring high hardness, including armor and tribological coatings.

Sorrell et al., and more recently Gunjishima et al., reported the directional solidification, microstructure and mechanical properties of several boride/carbide systems, including ZrB_2–ZrC,[1,7] B_4C–SiC[8] and B_4C–TiB_2.[9] These DSEs were grown by a float-zone (FZ) type method, leading to crystallographically and microstructurally well-oriented composites. In the float-zone method, a source material of the eutectic composition is passed through a hot zone at a well-defined rate, allowing for controlled melting and resolidification of the composite. Stubican[10] and Gunjishima,[9] among others,[11] showed that the solidification rate of non-oxide DSE materials has a direct influence on both the resulting microstructure and mechanical properties.

The B_4C–TiB_2 system (75 mol% B_4C),[9,11,12] which displays a lamellar-type eutectic microstructure, is a candidate for armor and tribological coatings where low density and high hardness are stringent requirements. Polotai et al.[11] demonstrated the formation of sub-micron scale B_4C–TiB_2 eutectic surface layers via laser processing of ceramic powders. Several oxide DSEs exhibit an increase in strength with decreasing microstructural scale,[6] and the same has been demonstrated in ZrC–ZrB_2 and ZrC–TiB_2 eutectics by Sorrel et al.[1] This study builds on the work of Polotai et al., investigating further the laser surface processing method, and determining the effect of microstructural scale on the indentation hardness of B_4C–TiB_2 eutectics.

* Corresponding author. Tel.: +1 814 865 9067; fax: +1 814 865 2326.
E-mail address: ecd10@psu.edu (E.C. Dickey).
[1] Current address: MRA Laboratories, Inc., 15 Print Works Drive, Adams, MA 01220, United States.

0955-2219/$ – see front matter © 2010 Elsevier Ltd. All rights reserved.
doi:10.1016/j.jeurceramsoc.2010.06.013

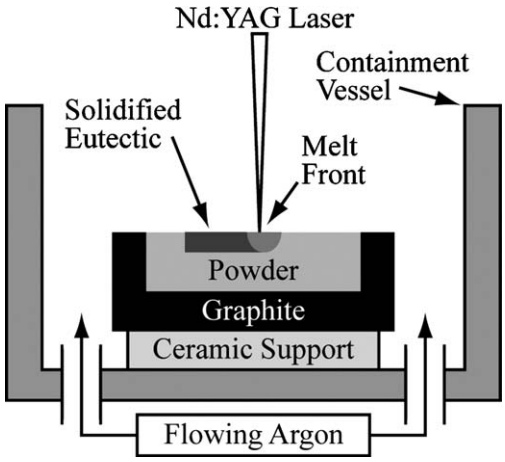

Fig. 1. Laser surface processing schematic.

2. Experimental procedure

Powders of B_4C (ESK, Germany, 96% pure) and TiB_2 (GE Advanced Ceramics, Wilton, CT, 93.5% pure) were combined in a mixture of 25 mol% TiB_2, corresponding to the pseudo-binary eutectic composition.[9,11,12] The powders were shaker-milled in ethanol for 24 h in a low-density polyethylene (LDPE) jar with yttria-stabilized zirconia milling media. The resulting slurry was then dried at 80 °C and passed through a centrifugal mill (Retsch, Germany) to produce a fine particle size suitable for hydraulic pressing. Powders were stored in a sealed LDPE jar and used within 1 week of production to minimize oxidation. Powders were pressed in a graphite crucible using a Carver hydraulic press (Carver Inc., Wabash, IN) and the green density was calculated via the known mass and measured volume of the pressed powder.

Prepared powders were melted and resolidified by scanning a 1064 nm Nd:YAG laser beam (Trumpf Inc., Farmington, CT) over the powder surface. A laser spot of approximately 4 mm in diameter was linearized with an oscillating mirror cycling at approximately 30 Hz. The linearized beam (approximately 12.7 mm long) was then scanned perpendicular to the oscillation direction at laser powers ranging from 500 to 1000 W, as illustrated in Fig. 1. The resolidified coupons were approximately square with 12.7 mm sides. Powder green density, laser power, and processing/resolidification rate were varied to determine relationships between processing variables and microstructure. Materials with the highest solidification rates were grown in the laser processing method described by Polotai et al.[11] No sample backheating was used during the current study, though backheating was used in the experiments performed by Polotai.

To prevent oxidation of the melt pool and resolidified material, processing was performed in an argon atmosphere. A sealed vessel was evacuated with a roughing pump (500 Torr) and backfilled to overpressure with high purity argon gas. This process was repeated three times, after which the top was removed from the vessel. Argon gas was flowed from the bottom of the vessel for the duration of processing and cooling. The containment vessel was evacuated and backfilled with argon as described each time the graphite crucible was changed.

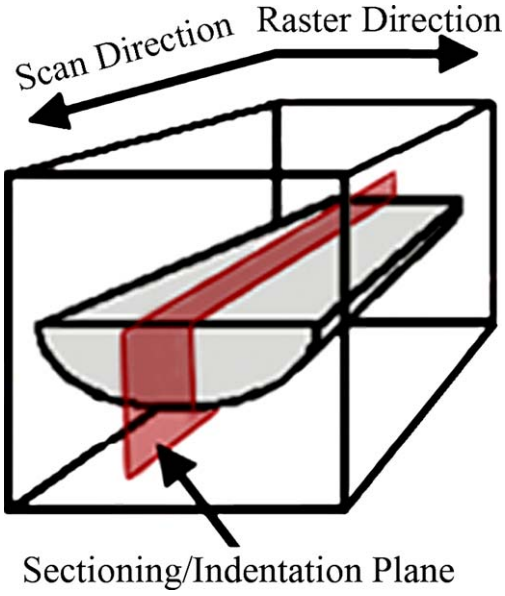

Fig. 2. Post-processing sample sectioning diagram.

The laser-processed coupons were removed from the crucibles and mounted in epoxy to aid in cross-sectioning and polishing. Samples were sectioned along a plane parallel to the growth direction as indicated in Fig. 2. Slices were cut from the remaining coupon with a high speed saw and cross-sectional surfaces were polished with diamond-embedded discs to 1 μm surface finish for observation in the Hitachi 3500-S (Hitachi, Japan) scanning electron microscope (SEM) and for Vickers hardness indentation.

In addition to laser-processed materials, samples of FZ-grown B_4C–TiB_2 were provided by P.I. Loboda and I. Bogmol from the National Technical University of Ukraine (Kiev Polytechnic Institute), grown with a crucible-free floating zone method.[12] Three separate materials were provided with growth rates of 3, 5 and 6 mm/min. These materials were polished to a surface roughness of 1 μm using a South Bay Tech 590 tripod polisher (South Bay Technologies, San Clemente, CA) and diamond lapping films (3M, St. Paul, MN).

Interlamellar spacing of the directionally solidified eutectic materials was measured as the average distance between lamellae. Vickers hardness indentations were performed on a Leica V-100 (Leica, Germany) indentation tester per ASTM C1327-03[13] at loads of 4.91, 9.81 and 19.62 N.

3. Results and discussion

3.1. Microstructure

Cross-sections of the laser-processed materials are analyzed with respect to the microstructural orientation and interlamellar spacing as a function of distance from the free surface. As is evident in Fig. 3, for samples processed at 0.42 mm/s, the orientation of the eutectic lamellae is inclined towards, but not perpendicular to, the sample surface, and there is only a small variation in the interlamellar spacing through the depth of the

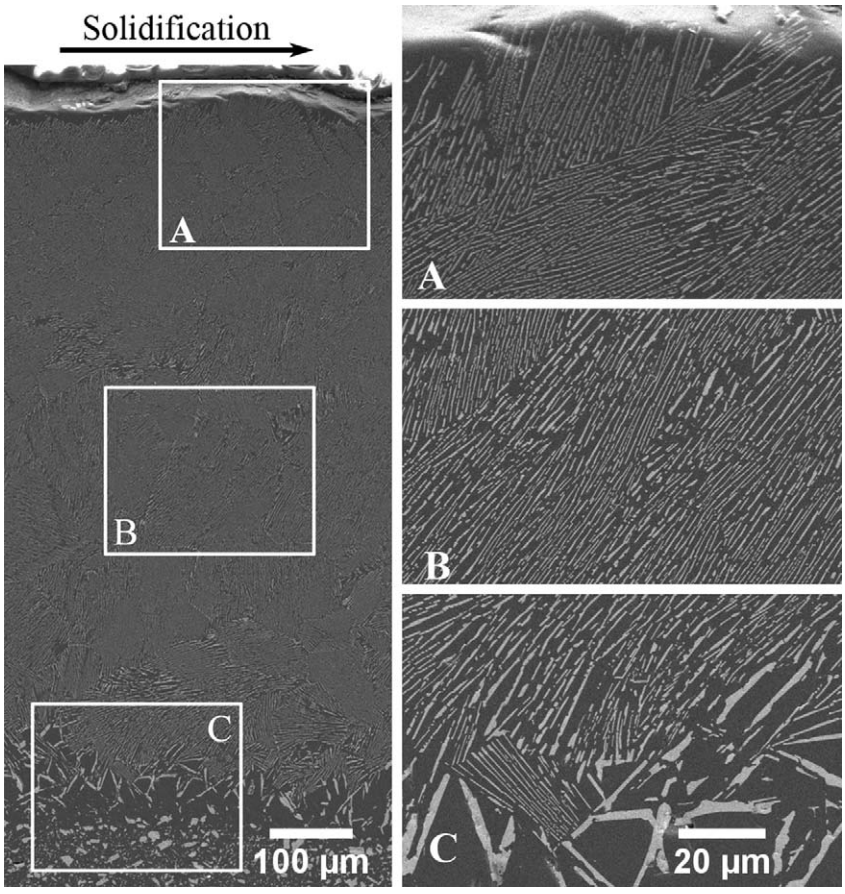

Fig. 3. Cross-sectional SEM image of a laser resolidified B_4C–TiB_2 eutectic coupon, processed at 0.42 mm/s.

eutectic layer. The microstructural orientation is similar to that found in other laser surface-processed eutectics, in which the bending of the eutectic microstructure is attributed to the shape of the melt front and subsequent solidification vector.[11,14,15] The variation in microstructural scale through the depth is attributed to the fact that the laser scanning direction is not collinear with the direction of growth, as indicated by the microstructural orientation. Larrea et al.[15] showed that the eutectic growth rate depends on the angle of the tangent to the solidification front, which varies through the depth. Additionally, Polotai et al.[11] found the shape of the liquid–solid interface is dependent on the laser scan rate, indicating the misorientation of the microstructure and the variation in interlamellar spacing will both increase with increasing laser scan rate.

Effects of the laser fluence and powder green density on the interlamellar spacing are summarized in Fig. 4. The interlamellar spacing is independent of both the green density of the starting powder and the incident laser energy, which is a function of both the laser fluence and scan speed. The data in Fig. 4 represent experiments performed at a laser scan rate of 0.42 mm/s and variable laser fluence by changing the laser power from 500 to 1000 W. Within the experimental error, no dependence of the interlamellar spacing on green density or laser fluence is observed, is observed. Further investigation will show that the solidification rate is primarily controlled by the laser scan speed.

Both Polotai[11] and Gunjishima[9] report an inverse correlation between the interlamellar spacing and eutectic solidification rate in B_4C–TiB_2 DSEs. Measurements from the current study are combined with these prior data in Fig. 5, which plots the interlamellar spacing as a function of the inverse square root of the growth rate, in accordance with the model proposed by Jackson and Hunt.[16]

According to the Jackson–Hunt model, increasing the solidification rate allows less time for the species to diffuse in the melt,

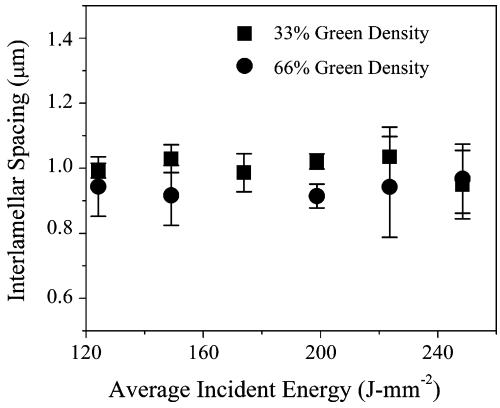

Fig. 4. Interlamellar spacing as a function of incident laser energy for various powder green densities. Error bars represent one standard deviation of at least 20 measurements.

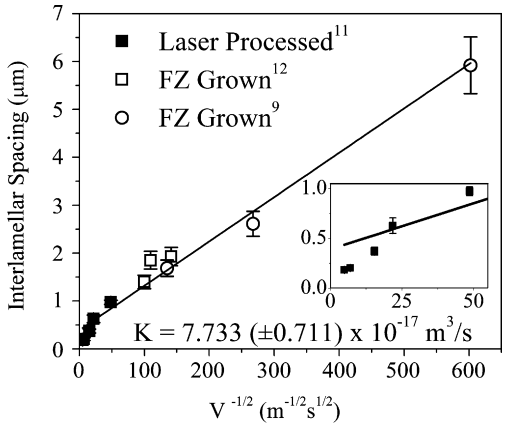

Fig. 5. Interlamellar spacing of B_4C–TiB_2 eutectics as a function of the inverse square root of solidification rate. Error bars (for this work) represent one standard deviation of 20 or more measurements of the interlamellar spacing.

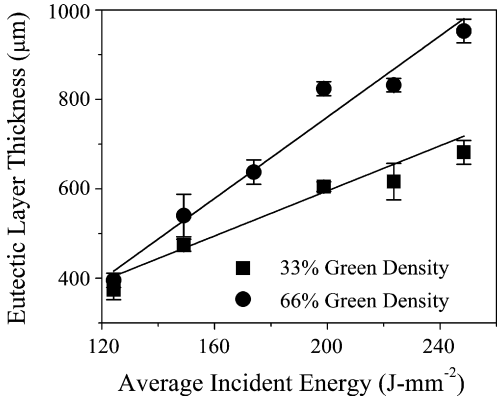

Fig. 6. Resolidified eutectic layer thickness as a function of incident laser energy for 33% and 66% powder green density. Error bars represent one standard deviation of 10 or more measurements of the resolidified eutectic thickness.

resulting in finer microstructural features, according to Eq. (1):

$$\lambda^2 V = K \tag{1}$$

in which λ is the interlamellar spacing, V is the eutectic growth rate, and K is a material-specific constant, which depends on Gibbs–Thompson coefficients, phase volume fractions, and liquid slopes, among other variables.[17] This general relationship, however, is predicted on the assumptions that the scale of the microstructure is much smaller than the diffusion distance of either species in the melt, i.e.:

$$\lambda \ll \frac{D}{V} \tag{2}$$

where D, for a binary eutectic, is the diffusion coefficient of the solute in the melt. In addition, Eq. (1) is strictly valid only when there is no significant constitutional undercooling. Theories based on the Trivedi, Magnin and Kurz (TMK) model[18–20] have been developed to predict eutectic solidification kinetics at high velocities.

Fig. 5, indeed, shows a clear linear relationship between the interlamellar spacing and inverse square root of the solidification velocity (Eq. (1)) for slower growth rates and a departure from this behavior at fast solidification velocities (>∼4.2 mm/s). At the lower growth rates, K can be calculated and used to predict the microstructural scale as a function of solidification rate. Including data from this study, K is calculated to be $(7.773 \pm 0.711) \times 10^{-17}\ m^3/s$, which is a good agreement with the values of 8.81×10^{-17} and $8.6 \times 10^{-17}\ m^3/s$ calculated by Polotai[11] and Gunjishima,[9] respectively. At velocities greater than 4.2 mm/s a significant departure from linear behavior is observed in which the interlamellar spacing decreases more strongly with increasing solidification velocity. Data points which depart from the Jackson–Hunt model (high solidification rate) were excluded from the linear fit in Fig. 5 and subsequent calculation of K.

The effects of processing parameters on the thickness of the resolidified eutectic layer are also summarized in Fig. 6. In these experiments, the powder green density and laser fluence are varied while the laser scan speed is kept constant at 0.42 mm/s.

The relationship between the thickness of the resolidified eutectic layer and the incident beam energy is nearly linear, as would be expected since increasing the incident beam energy results in a concomitant increase in absorbed energy. The maximum eutectic layer thicknesses are 682 ± 26.6 and $953 \pm 26.6\ \mu m$ for 33% and 66% powder green densities, respectively.

The dependence of the eutectic depth as a function of green density is more complex in that the density affects both the absorbance and the thermal conductivity of the green powders. Prior work has shown that during laser irradiation of porous powders, the absorption depth decreases with increasing green density, since the absorption coefficient of the gas phase is, in general, less than that of the solid.[21] The thermal diffusion of the absorbed energy, however, depends on the thermal conductivity of the sample. Using a rule of mixtures for TiB_2, B_4C and Ar, we estimate the thermal conductivity of the 33% green density powder to be $9.0\ W\ m^{-1}\ K^{-1}$ as compared to a value for 66% density of $18.1\ W\ m^{-1}\ K^{-1}$. Even though the laser absorption is more confined to the surface region in the higher green density samples, the larger thermal conductivity leads to a greater melt depth. This simplified analysis provides a qualitative description of the effects of powder green density on the eutectic depth. A quantitative analysis would need to consider the evolution of the eutectic microstructure and other effects, such as convective flow in the melt.

While thicker eutectic layers can be produced by increasing the incident laser energy, this approach is limited due to formation of porosity. Fig. 7 shows an area containing pores and a crack in a resolidified coupon processed at 0.42 mm/s. The number and size of pores was found to increase with increasing laser fluence, indicating the pores may be linked to gas trapped in the green powders prior to solidification[22] or the formation of boron gas via decomposition of B_4C.[23] Adequate data has not been collected to correlate pore size or pore density to specific laser processing parameters. Cracking in the resolidified materials was also observed, often in conjunction with porous areas, indicating the pores may serve as stress concentrators and nucleation sites for cracks upon cooling.

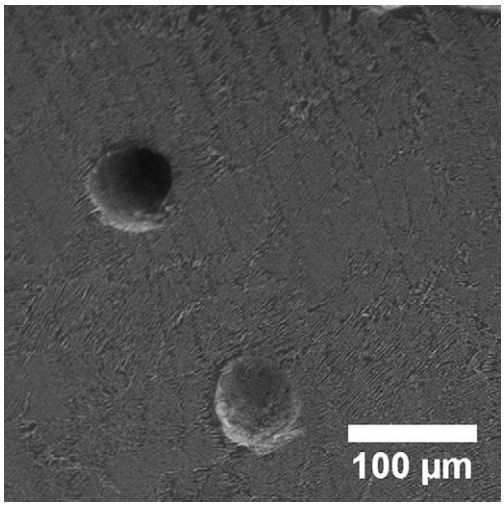

Fig. 7. Pores in eutectic layer processed at 0.42 mm/s.

3.2. Microstructure and Vickers hardness

Fig. 8 shows the relationship between eutectic interlamellar spacing and Vickers indentation hardness at a load of 9.81 N. As the eutectic processing rate is increased and the microstructural scale decreases, the Vickers indentation hardness increases substantially. At low solidification rates (0.05–0.1 mm/s), the interlamellar spacing of the composites ranges from 2 to 2.8 μm, and the hardness from 21 to 23 GPa, respectively. At the highest solidification rate of 42 mm/s, corresponding to an interlamellar spacing of 0.18 μm, the Vickers hardness reaches 32 GPa.

The increase in indentation hardness is similar to the behavior first observed by Hall and Petch regarding the strengthening of metals and ceramics with decreasing grain size.[24,25] Fig. 8, however, illustrates a near linear relationship between the microstructural scale and the indentation hardness, departing from the inverse square root relationship generally accepted for dislocation impedance by interfaces.

To further investigate the indentation behavior, the load-dependent hardness of the eutectics is investigated for different

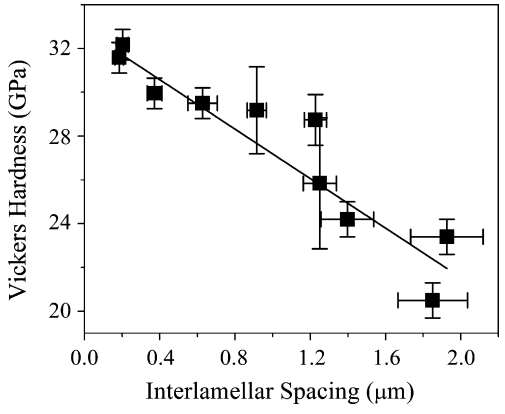

Fig. 8. Vickers indentation hardness of B_4C–TiB_2 eutectic as a function of interlamellar spacing. Error bars represent one standard deviation of 20 or more measurements of interlamellar spacing and 10 or more measurements of indentation hardness.

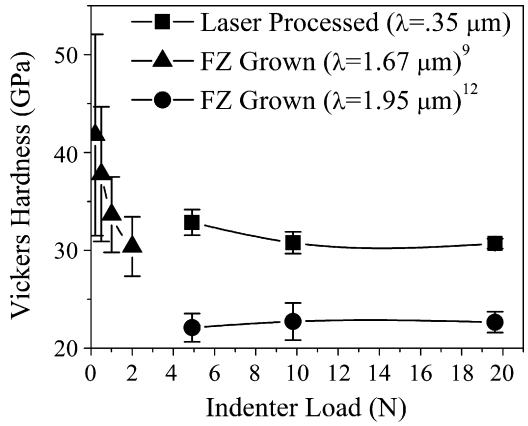

Fig. 9. Load-dependent hardness of B_4C–TiB_2 eutectics. Error bars (from this work) represent one standard deviation of 10 or more Vickers hardness indentations.

values of interlamellar spacing. Fig. 9 illustrates that the materials processed at high speed ($\lambda = 0.35$ μm) are approximately 35% harder than those processed at much slower speeds ($\lambda = 1.95$ μm) over a large range of indenter loads. Additional data is reported from Gunjishima et al. although hardness measurements were made at different loads than the current work.

Also evident from the combined data in Fig. 9 is a load-dependent hardness. Some authors have found, specifically in brittle ceramics, that a plateau in the load–hardness curve indicates a transition from dislocation to fracture deformation modes.[26] Under indentation loading, boron carbide is found to transition from single- to nanocrystalline,[27,28] so it is unclear whether the aforementioned load-hardness analyses are applicable. Authors have found basal slip to be prevalent in TiB_2,[29] but further observation of deformed material is required to determine the deformation mechanisms of each phase in the composite.

4. Conclusions

B_4C–TiB_2 eutectic surface layers are formed via directional solidification of powders by a high power Nd:YAG laser. The resulting eutectic microstructures have uniform lamellar spacings through the thickness of the resolidified layer and are well adhered to the underlying sintered composite. The increased processing rate afforded by the direct energy of the laser beam allows for vastly increased processing speeds (up to 42 mm/s) as compared to the traditional float-zone method. As the processing rate is increased, the interlamellar spacing of the eutectic decreases in proportion to the inverse square root of the eutectic solidification speed up to processing rates of 4.2 mm/s. Beyond this solidification rate, the scale of the eutectic microstructure deviates from the traditional Jackson–Hunt theory and decreases rapidly with increased solidification rate. While the interlamellar spacing is only a function of the laser scan rate, the thickness of the resolidified eutectic layer can be increased with both laser power and the green density of the processed powder. The depth of the eutectic layer becomes limited by thermal decomposition of the B_4C as the laser fluence is increased.

The decreased interlamellar spacing afforded by the fast solidification velocities leads to a pronounced increase in the Vickers indentation hardness of the eutectics, with an approximate inverse linear relationship. For the smallest microstructures produced (180 nm interlamellar spacing), the Vickers indentation hardness is 32 GPa at 9.8 N (well into the load-independent regime). The results show that the microstructure and indentation properties of the eutectic surface layers can be tailored with the solidification parameters.

Acknowledgements

The authors would like to thank I. Bogmol, T. Nishimura, O. Vasylkiv, Y. Sakka and P.I. Loboda of the National Technical University of Ukraine (Kiev Polytechnic Institute) for generously providing FZ-grown samples of B_4C–TiB_2 eutectic.

References

1. Sorrell CC, Stubican VS, Bradt RC. Mechanical properties of ZrC–ZrB_2 and ZrC–TiB_2 directionally solidified eutectics. *Journal of the American Ceramic Society* 1986;**69**:317–21.
2. Deng H, Dickey EC, Paderno Y, Paderno V, Filippov V, Sayir A. Crystallographic characterization and indentation mechanical properties of LaB_6–ZrB_2 directionally solidified eutectics. *Journal of Materials Science* 2004;**39**:5987–94.
3. Mazerolles L, Perriere L, Lartigue-Korinek S, Piquet N, Parlier M. Microstructures, crystallography of interfaces, and creep behavior of melt-growth composites. *Journal of the European Ceramic Society* 2008;**28**:2301–8.
4. Ashbrook RL. Directionally solidified ceramic eutectics. *Journal of the American Ceramic Society* 1977;**60**:428–35.
5. Dickey EC, Frazer CS, Watkins TR, Hubbard CR. Residual stresses in high-temperature ceramic eutectics. *Journal of the European Ceramic Society* 1999;**19**:2503–9.
6. Llorca J, Orera VM. Directionally solidified eutectic ceramic oxides. *Progress in Materials Science* 2006;**51**:711–809.
7. Sorrell CC, Beratan HR, Bradt RC, Stubican VS. Directional solidification of (Ti,Zr) carbide–(Ti,Zr) diboride eutectics. *Journal of the American Ceramic Society* 1984;**67**:190–4.
8. Gunjishima I, Akashi T, Goto T. Characterization of directionally solidified B_4C–SiC composites prepared by a floating zone method. *Materials Transactions* 2002;**43**:2309–15.
9. Gunjishima I, Akashi T, Goto T. Characterization of directionally solidified B_4C–TiB_2 composites prepared by a floating zone method. *Materials Transactions* 2002;**43**:712–20.
10. Stubican VS, Bradt RC. Directional solidification of nonoxide eutectics. U.S. Army Research Office Report; 1980 [publicly available].
11. Polotai AV, Foreman JF, Dickey EC, Meinert K. Laser surface processing of B_4C–TiB_2 eutectic. *International Journal of Applied Ceramic Technology* 2008;**5**:610–7.
12. Bogomol I, Nishimura T, Vasylkiv O, Sakka Y, Loboda P. Microstructure and high-temperature strength of B_4C–TiB_2 composite prepared by a crucibleless zone melting method. *Journal of Alloys and Compounds* 2009;**485**:677–81.
13. *ASTM C1327 – 08 standard test method for vickers indentation hardness of advanced ceramics*. ASTM; 2008.
14. Larrea A, Orera VM, Merino RI, Peña JI. Microstructure and mechanical properties of Al_2O_3–YSZ and Al_2O_3–YAG directionally solidified eutectic plates. *Journal of the European Ceramic Society* 2005;**25**:1419–29.
15. Larrea A, de la Fuente GF, Merino RI, Orera VM. ZrO_2–Al_2O_3 eutectic plates produced by laser zone melting. *Journal of the European Ceramic Society* 2002;**22**:191–8.
16. Jackson KA, Hunt JD. Lamellar and rod eutectic growth. *Transactions of the Metallurgical Society of AIME* 1966;**236**:1129–42.
17. Kurz W, Fisher DJ. *Fundamentals of solidification*. Brookfield, VT: Trans Tech Publications; 1989.
18. Trivedi R, Magnin P, Kurz W. Theory of eutectic growth under rapid solidification conditions. *Acta Metallurgica* 1987;**35**:971–80.
19. Kurz W. Eutectic growth under rapid solidification conditions. *Metallurgical and Materials Transactions A: Physical Metallurgy and Materials Science* 1991;**22**:3051.
20. Wei B, Herlach DM, Sommer F. Rapid eutectic growth of undercooled metallic alloys. *Journal of Materials Science Letters* 1993;**12**:1774–7.
21. McVey RW, Melnychuk RM, Todd JA, Martukanitz RP. Absorption of laser irradiation in a porous powder layer. *Journal of Laser Applications* 2007;**19**:214–24.
22. Triantafyllidis D, Li L, Stott FH. Mechanisms of porosity formation along the solid/liquid interface during laser melting of ceramics. *Applied Surface Science* 2003;**208**:458–62.
23. Hildenbrand DL, Hall WF. The decomposition pressure of boron carbide and the heat of sublimation of boron. *Journal of Physical Chemistry* 1964;**68**:989–93.
24. Hall EO. The deformation and ageing of mild steel. III Discussion of results. *Proceedings of the Physical Society, Section B* 1951;**64**:747–53.
25. Petch NJ. The cleavage strength of polycrystals. *Journal of the Iron and Steel Institute* 1953;**174**:25–9.
26. Quinn JB. Indentation brittleness of ceramics: a fresh approach. *Journal of Materials Science* 1997;**32**:4331–6.
27. Ge D, Domnich V, Juliano T, Stach EA, Gogotsi Y. Structural damage in boron carbide under contact loading. *Acta Materialia* 2004;**52**:3921–7.
28. Domnich V, Gogotsi Y, Trenary M, Tanaka T. Nanoindentation and Raman spectroscopy studies of boron carbide single crystals. *Applied Physics Letters* 2002;**81**:3783–5.
29. Vahldiek FW, Mersol SA. Slip and microhardness of IVa to VIa refractory materials. *Journal of the Less Common Metals* 1977;**55**:265–78.